Flow and Heat Transfer in a Non-Newtonian Dusty Fluid with Particle Suspension

Anitha V

Department of Mathematics, Sir M. V. Government Science College, Bommanakatte, Bhadravathi, Karnataka – 577 302, India
Email: *anumurthy20[at]gmail.com*

Abstract: *An analysis is carried out to study the flow and heat transfer characteristics of an non-Newtonian fluid, namely, the upper convected Maxwell (UCM) fluid over a stretching sheet in a porous medium. The stretching velocity and the temperature at the surface are assumed to vary linearly with the distance from the origin. The flow is induced by the infinite elastic sheet which is being stretched in its own plane. Using a similarity transformation, the governing non-linear partial differential equations of the model problem are transformed into coupled non-linear ordinary differential equations and the equations are solved numerically by a second order finite difference implicit method. Comparisons with previously published works are presented as special cases. Furthermore, the effects of the physical parameters on the fluid velocity, the velocity of the dust particle, the density of the dust particle, the fluid temperature, the dust-phase temperature, the skin friction, and the wall-temperature gradient are presented through tables and graphs. One of the important observations is that, Maxwell fluid reduces the wall-shear stress. The results obtained for the flow and heat transfer characteristics reveal many interesting behaviors that warrant further study on the non-Newtonian fluid phenomena, especially the dusty UCM fluid phenomena.*

Keywords: Heat transfer, Porous medium, UCM fluid, dusty fluid, fluid particle interaction, numerical solution, stretching sheet

1. Introduction

The heat transfer due to a continuously moving surface through an ambient liquid is one of the important areas of current research due to its extensive application in broad spectrum of science and engineering disciplines, for instance, in chemical engineering processes like metallurgical process and polymer extrusion process involving cooling of a molten liquid being stretched into a cooling system. The fluid mechanical properties desired for an outcome of such a process would mainly depend on two aspects, one is the cooling liquid used and the other is the rate of stretching. Liquids of non-Newtonian characteristics, which are electrically conducting, can be opted as a cooling liquid as the flow and the heat transfer can be regulated by some external agency. Rate of stretching is very important as rapid stretching results in sudden solidification there by destroying the expected properties of the outcome. This is a fundamental problem that arises frequently in many practical situations such as polymer extrusion process; other processes like drawing; annealing and tinning of copper wires; continuous stretching; rolling and manufacturing of plastic films and artificial fibers; heat treated materials traveling on conveyer belts; glass blowing; crystal growing; paper production and so on. Sakiadis [1] was the first among the others to study the boundary layer flow generated by a continuous solid surface moving with constant velocity. Crane [2] extended the work of Sakiadis [1]and analyzed a steady two-dimensional boundary layer flow caused by a stretching sheet moving with a velocity linearly varying with the distance from a fixed point on the sheet. Many investigators have extended the work of Crane to study heat and mass transfer under different physical situations [3-7].

Since the analyses of fluid flow and heat transfer in the presence of porous medium has many applications in polymer industry. In this view of applications, Subhas & Veena [8] studied the flow of viscoelastic fluid over an impermeable stretching surface with saturated porous medium and found that the increase in the permeability of the porous medium leads to the deceleration of the flow. Chakrabarti & Gupta [9] analyzed the electrically conducting Newtonian fluid flow and heat transfer past a porous stretching sheet and have obtained the analytical solution for the flow and numerical solution for the heat transfer problem. Zheng et al. [10] investigated the nanofluid flow over a stretching sheet with porous medium in the presence of radiation, velocity slip and temperature jump. And also, they have compared their numerical results with the analytical solutions and found that they are in good agreement. Prasad et al. [11] presented the influence of reaction rate on the transfer of chemically reactive species in the non-Newtonian fluid flow over a porous stretching sheet and found that the decreasing chemical reaction reduces the thickness of the concentration boundary layer and increases the mass transfer rate. Khan et al. [12] studied the flow and heat transfer properties of the thin film second-grade fluid over a stretching sheet with porous medium in the presence of viscous dissipation. Similarly, many authors have studied the several types of electrically conducting non-Newtonian fluid flow and heat transfer over a linear or non-linear stretching sheet [13-20].

All the above investigators restrict their analyses to the flow induced by a stretching sheet in the absence of fluid-particle suspension. The analysis of two-phase flow in which solid spherical particles are distributed in a fluid are of interest in a wide range of technical problems such as flow through packed beds, sedimentation, environmental pollution, centrifugal separation of particles and blood rheology. The study of the fluid-particle suspension flow is important in determining the particle accumulation and impingement of the particle on the surface. Saffman [21] investigated the stability of the laminar flow of a dusty gas in which the dust particles are uniformly distributed. Datta and Mishra [22] studied the dusty fluid flow over a semi-infinite flat plate.

Vajravelu and Nayfeh [23] analyzed the hydromagnetic flow of dusty fluid over a stretching sheet with the effect of suction. Further Xie et al. [24] have extended the work of Datta and Mishra [22] to study the hydrodynamic stability of a particle-laden flow in growing flat plate boundary layer. Recently, Vajravelu et al.[25] studied the effects of variable viscosity and variable thermal conductivity on the hydromagnetic fluid-particle suspension flow and heat transfer over a stretching sheet. In these studies, the physical properties of the ambient fluid were assumed to be constant. However, it is known that these physical properties of the ambient fluid may change with temperature [26-27]. For lubricating fluids, heat generated by internal friction and the corresponding rise in the temperature affects the thermal conductivity of the fluid so it can no longer be assumed constant. The increase of temperature leads to increase in the transport phenomena by reducing the thermal conductivity across the thermal boundary layer due to which the heat transfer at the wall is also affected. Therefore to predict the flow and heat transfer rates, it is necessary to take variable thermal conductivity of the fluid into account. Available literature on variable thermal conductivity and fluid–particle interaction shows that combined work has not been carried out for UCM fluid over a stretching sheet.

Motivated by these analyses, in the present paper, the authors study the flow and heat transfer of a dusty non-Newtonian UCM fluid over a stretching sheet in a porous medium. This is in contrast to the work of Vajravelu and Nayfeh [22], where Newtonian fluid with constant thermal conductivity was considered. Because of the non-Newtonian rheology, the fluid-particle interaction, the momentum and energy equations for both the fluid and the dust phase are coupled and highly non-linear partial differential equations (PDEs). These PDEs are converted to couple, non-linear ordinary differential equations (ODEs) by similarity variables. Because of the complexity and the non-linearly, we propose to solve these equations by a second order finite difference scheme known as the Keller-box method. The effects of pertinent parameters on the velocity and temperature fields, the skin friction coefficient and the local Nusselt number are presented in graphs and tables. It is believed that the results obtained in the present study will provide useful information for applications and will complement to the results in the literature.

2. Mathematical Formulation

Consider a steady two-dimensional, boundary layer flow of a viscous incompressible and dusty non-Newtonian fluid (namely, UCM fluid) over a horizontal stretching sheet in a porous medium with a stretching velocity $U_w(x) = bx,$

and prescribed surface temperature $T_w(x) = A(x/l)$; where $b > 0$ is the stretching velocity rate, l is the reference length scale, and A is a constant. The sheet is coinciding with the plane $y = 0$, with the flow being confined to $y > 0$. Two equal and opposite forces are introduced along the *x*-axis, so that the sheet is stretched, keeping the origin fixed (see Fig. 1).
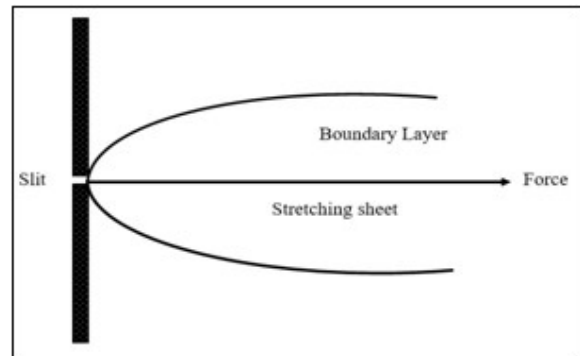

Figure 1: Physical model and co-ordinate system

The thermo-physical fluid properties are assumed to be isotropic and constant, except for the thermal conductivity which is assumed to vary as a function of temperature in the following form (see [26])

$$K(T) = K_\infty \left(1 + \frac{\varepsilon}{\Delta T}(T - T_\infty) \right), \qquad (1)$$

where $K(T)$ is the temperature dependent fluid thermal conductivity, K_∞ is the thermal conductivity far away from the slit, $\varepsilon = (K_w - K_\infty)/K_\infty$ is a small parameter known as the variable thermal conductivity parameter, K_w is the thermal conductivity at the surface, $\Delta T = T_w - T_\infty$, T_w is the surface temperature, and T_∞ is the ambient temperature. Further, the fluid and the dust particle clouds are suppose to be static at the beginning. The dust particles are assumed to be spherical in shape and uniform in size and density of the dust particle is taken as a constant throughout the flow. Under these conditions, the basic boundary-layer equations for continuity, conservation of mass (with no pressure gradient), and energy for clear UCM fluid as well as dusty fluid can be written as

$$\frac{\partial u}{\partial x} + \frac{\partial v}{\partial y} = 0, \qquad (2)$$

$$u\frac{\partial u}{\partial x} + v\frac{\partial u}{\partial y} + \lambda\left(u^2\frac{\partial^2 u}{\partial x^2} + v^2\frac{\partial^2 u}{\partial y^2} + 2uv\frac{\partial^2 u}{\partial x\partial y} \right) = v\frac{\partial^2 u}{\partial y^2} - \frac{v}{K'}u - \frac{\rho_p}{\rho\tau}(u - u_p), \qquad (3)$$

$$u_p\frac{\partial u_p}{\partial x} + v_p\frac{\partial u_p}{\partial y} = \frac{1}{\tau}(u - u_p), (4)$$

$$\frac{\partial}{\partial x}(\rho_p u_p) + \frac{\partial}{\partial y}(\rho_p v_p) = 0, \quad (6)$$

$$u_p\frac{\partial v_p}{\partial x} + v_p\frac{\partial v_p}{\partial y} = \frac{1}{\tau}(v - v_p), (5)$$

$$u\frac{\partial T}{\partial x} + v\frac{\partial T}{\partial y} = \frac{\partial}{\partial y}\left(\frac{K(T)}{\rho c_p}\frac{\partial T}{\partial y} \right) + \frac{\rho_p c_s}{\rho\gamma_T c_p}(T_P - T),$$

$$(7)$$

Volume 10 Issue 9, September 2021

$$u_p \frac{\partial T_p}{\partial x} + v_p \frac{\partial T_p}{\partial y} = -\frac{1}{\gamma_T}(T_P - T). \quad (8)$$

where (u, v) and (u_p, v_p) are the velocity components of the fluid and dust particle phases along the x and y axes, respectively; K' is the permeability of the porous medium and ρ is the density of the fluid. Here $\tau = 1/k$ is the relaxation time of particles, k is the Stokes' constant $(= 6\pi\mu D)$, μ is the coefficient of viscosity and D is the average radius of the dust particles. Further, σ is the electrical conductivity, λ is the relaxation time and ρ_p is the mass of the dust particles per unit volume of the fluid. T

and T_p are respectively, the temperatures of the fluid and the dust phase particles. Further, c_p and c_s are, respectively, the specific heat capacity of the fluid and the specific heat capacity of the dust particles, γ_T is the temperature relaxation time $(= 3 \Pr \gamma_p c_p / 2c_p)$; γ_p is the velocity relaxation time $(= 1/k)$; and $\Pr$ is the usual Prandtl number. The last term in "Eq. (3)"represents the force due to the relative motion between the fluid and the dust particles. In deriving these equations the Stokesian drag force is considered for the interaction between the fluid and the particle phases. The appropriate boundary conditions on velocity and temperature are

$$u = U_w(x) = bx, \quad v = 0, \quad T = T_w = A(x/l) \quad at \quad y = 0,$$
$$u \to 0, \, u_p \to 0, \, v_p \to v, \, \rho_p \to k\rho, \, T \to T_\infty, \, T_p \to T_\infty \quad as \quad y \to \infty. \quad (9)$$

To convert the governing equations into a set of similarity equations, we introduce the following new variables

$$\eta = \sqrt{\frac{b}{v}}y, \, u = bx f'(\eta), \quad v = -\sqrt{bv} f(\eta), \, u_p = bx F(\eta), \, v_p = \sqrt{bv}G(\eta),$$

$$\rho_r = H(\eta), T - T_\infty = (T_w - T_\infty)\theta(\eta), \, T_P - T_\infty = (T_w - T_\infty)\theta_P(\eta), \quad T_w - T_\infty = A(x/l), \quad (10)$$

Where η is the similarity variable and prime denotes differentiation with respect to η, $\rho_r = \rho_p / \rho$ is the relative density, $f, F, G, H, \theta, \theta_p$ are dimensionless quantities and v is the kinematic viscosity. Substituting "(10)" into "(3) - (8)", we obtain the following coupled non-linear ordinary differential equation

$$f''' + ff'' - f'^2 + \beta_1(2ff'f'' - f^2 f''') - K_1 f' + H\beta(F - f') = 0,$$

$$GF' + F^2 + \beta(F - f') = 0,$$

$$GG' + \beta(f + G) = 0,$$

$$GH' + HG' + FH = 0,$$

$$((1 + \varepsilon\theta)\theta')' - \Pr \begin{vmatrix} f' & \theta' \\ f & \theta \end{vmatrix} + \frac{2}{3}\beta H(\theta_P - \theta) = 0, \quad (11)$$

$$2F\theta_P + G\theta_P' + L_0\beta(\theta_P - \theta) = 0,$$

along with the boundary conditions

$$f' = 1, \quad f = 0, \quad \theta = 1 \quad at \quad \eta = 0,$$
$$f' \to 0, \, F \to 0, \, G \to -f, \, H \to k,$$
$$\theta \to 0, \, \theta_P \to 0 \quad as \quad \eta \to \infty, \quad (12)$$

where $K_1 = v/K'b$ is the permeability parameter, $\beta = 1/b\tau$ is the fluid-particle interaction parameter, $\beta_1 = \lambda b$ is the Maxwell parameter, and $L_0 = \tau/\gamma_T$ is the temperature relaxation parameter. The physical quantities of interest are the skin friction coefficient C_f and the local Nusselt number Nu_x which are defined by

$$C_f = \frac{\tau_w}{\rho_\infty U_w^2/2}, \, Nu_x = \frac{xq_w}{k_\infty(T_w - T_\infty)}, \quad (13)$$

where τ_w is the surface shear stress and q_w. The surface heat flux are given by

$$\tau_w = \mu_\infty \left(\frac{\partial u}{\partial y}\right)_{y=0}, \quad q_w = -K_\infty \left(\frac{\partial T}{\partial y}\right)_{y=0}. \quad (14)$$

Using the similarity variables (10), we obtain

$$\frac{1}{2}C_f \text{Re}_x^{1/2} = f''(0), \text{ and} \frac{Nu_x}{\text{Re}_x^{1/2}} = -\theta'(0), \quad (15)$$

where $\text{Re}_x = U_w x / v$ is the local Reynolds number.

2.1 Exact solutions for some special cases:

Here we present exact solutions in certain special cases. Such solutions are useful and serve as a baseline for comparison with the solutions obtained via numerical schemes.

(a) No permeability of the porous medium and no fluid-particle interaction:

In the limiting case of $\beta_1 = 0$ and $\beta = 0$, the MHD boundary layer flow and heat transfer problem degenerates. In this case the results of the present work are compared with the exact solution of Chakrabarti and Gupta [9] and are presented in Table1.From this table it is obvious that the numerical solutions are in close agreement with the exact ones of [9],[2] and [3].

(b)No magnetic field but in the presence of fluid-particle interaction:

In the absence of Maxwell parameter, the system in (11) reduces to those of Vajravelu et al. [25], when no variable

thermo-physical properties are considered. Further, when the energy transfer and magnetic field are not considered, equations in(11) reduce to those of Vajravelu and Nayfeh [23].Further, when the variable thermal conductivity parameter, and the Maxwell parameter are absent, the analytical solutions are obtained via perturbation technique for small values of fluid–particle interaction parameter. For small values of fluid–particle interaction parameter let us perturb the flow and heat transfer fields as

$$f = f_0 + \beta f_1 + 0\left(\beta^2\right),$$
$$F = F_0 + \beta F_1 + 0\left(\beta^2\right),$$
$$G = G_0 + \beta G_1 + 0\left(\beta^2\right),$$
$$H = H_0 + \beta H_1 + 0\left(\beta^2\right),$$
$$\theta = \theta_0 + \beta \theta_1 + 0\left(\beta^2\right),$$
$$\theta_p = \theta_{p0} + \beta \theta_{p1} + 0\left(\beta^2\right),$$

(16)

where the perturbations f_1, F_1, G_1 and H_1 are small compared with the mean or the zeroth-order quantities. With the help of equations in (16), the system of equations (11) and the boundary conditions (12) become

$$\theta_1'' + Pr\left(f_0\theta_1' - f_0'\theta_1\right) = \frac{2}{3}H_0\left(\theta_0 - \theta_{p0}\right) - Pr\left(f_1\theta_0' - f_1'\theta_0\right),$$
$$G_0\theta_{p1}' + F_0\theta_{p1} = -F_1\theta_{p0} - G_1\theta_{p0}' + L_0\left(\theta_0 - \theta_{p0}\right),$$
$$f_1' = 0, \quad f_1 = 0, \quad \theta_1 = 0 \qquad \eta = 0,$$
$$f_1' \to 0, \quad F_1 \to 0, \quad G_1 \to -f_1, \quad H_1 \to k, \quad \theta_1 \to 0, \quad \theta_{p1} \to 0 \quad \text{as} \quad \eta \to \infty,$$

(18)

to the first-order.

The exact solutions (in terms of Kummer's function ϕ) for the zeroth-order velocity components f_0, G_0, F_0, particle density H_0 and temperature θ_0 are

$$f_0 = A_1 + B_1\exp\left(-\delta\eta\right), \quad F_0 = 0, \quad G_0 = -A_1, \quad H_0 = k,$$

$$f_1 = \left\{-kB_1/\left(A_1\delta - B_1\delta + 2Mn\right)\right\}e^{-\delta\eta} + \delta\eta e^{-\delta\eta} - 1, \qquad F_1 = -\left(B_1/A_1\right)e^{-\delta\eta},$$

$$G_1 = -\left(B_1/A_1\right)e^{-\delta\eta} - \left\{-kB_1/\left(A_1\delta - B_1\delta + 2Mn\right)\right\}, \qquad H_1 = 0, \qquad \theta_{p1} = -\frac{L_0}{G_0}\int_\eta^\infty \theta_0\left(z\right)dz,$$

(20)

where A_1, B_1, δ are constants. The solution θ_1 may be obtained by solving the inhomogeneous equation it satisfies, using the standard variation of parameter method. The results for various values of K_1, Pr and β_1 are compared with the available results in the literature, and are shown in Table2. The results in tables 1 and 2 reveal very good agreement between our numerical results and the available results in the literature.

$$f_0''' + f_0 f_0'' - \left(f_0'\right)^2 - Mn f_0' = 0,$$
$$G_0 F_0' + F_0^2 = 0,$$
$$G_0 G_0' = 0,$$
$$G_0 H_0' + H_0 G_0' + F_0 H_0 = 0,$$
$$\theta_0'' + Pr\left(f_0\theta_0' - f_0'\theta_0\right) = 0,$$
$$2F_0\theta_{p0} + G_0\theta_{p0}' = 0,$$

(17)

$$f_0' = 1, \quad f_0 = 0, \quad \theta_0 = 1 \qquad \eta = 0,$$
$$f_0' \to 0, \quad F_0 \to 0, \quad G_0 \to -f_0,$$
$$H_0 \to k, \quad \theta_0 \to 0, \quad \theta_{p0} \to 0 \quad \text{as} \quad \eta \to \infty,$$

To the zeroth- order and

$$f_1''' + f_1 f_0'' + f_0 f_1'' - 2f_0' f_1' - Mn f_1' + H_0\left(F_0 - f_0'\right) = 0,$$
$$G_0 F_1' + G_1 F_0' + 2F_0 F_1 + F_0 - f_0' = 0,$$
$$G_0 G_1' + G_0' G_1 + f_0 + G_0 = 0,$$
$$G_0 H_1' + H_0' G_1 + H_0 G_1' + G_0' H_1 + F_0 H_1 + H_0 F_1 = 0,$$

$$\theta_0 = \exp\left(-\frac{Pr}{\delta}\eta\right)\frac{\phi\left(\frac{Pr}{\delta^2}-1, \ 1+\frac{Pr}{\delta^2}, -\frac{Pr}{\delta^2}e^{-\delta\eta}\right)}{\phi\left(\frac{Pr}{\delta^2}-1, \ 1+\frac{Pr}{\delta^2}, -\frac{Pr}{\delta^2}\right)}, \quad \theta_{p0} = 0$$

(19)

where $A_1 = 1/\delta$, $B_1 = -1/\delta$, $\delta = \sqrt{1+K_1}$.

Similarly the exact solutions for the first-order velocity components, first-order particle density and first-order temperature, satisfying the differential equations and the boundary conditions are

3. Numerical Procedure

The system (11) is coupled and highly nonlinear. Exact analytical solutions are not possible for the complete set of equations and, therefore, we use the efficient numerical method with second order finite difference scheme known as the Keller–box method [28, 29]. The coupled non-linear ordinary differential equations (11) and (12) are reduced to a system of nine first order equations with nine unknowns, by

Volume 10 Issue 9, September 2021

assuming $f = f_1$, $f' = f_2$, $f'' = f_3$, $\theta = \theta_1$, $\theta' = \theta_2$. To solve this system of equations we require nine initial conditions while we have only two initial conditions $f(0)$, $f'(0)$ on f and one initial condition $\theta(0)$ on θ The other six initial conditions $f''(0)$, $F(0)$, $G(0)$, $H(0)$, $\theta'(0)$ and $\theta_p(0)$ are not known. However, the values of $f'(\eta)$, $F(\eta)$, $G(\eta)$, $H(\eta)$, $\theta(\eta)$ and $\theta_p(\eta)$ are known as $\eta \to \infty$. We employ the Keller-box scheme and use the six known boundary conditions to produce six unknown initial conditions at $\eta = 0$. To select η_∞, we begin with some initial guess values and solve the boundary value problem with some particular set of parameters to obtain $f''(0)$, $F(0)$, $G(0)$, $H(0)$, $\theta'(0)$ and $\theta_p(0)$. Thus, we start with the initial approximations as $f''(0) = \delta_1, F(0) = \delta_2, G(0) = \delta_3, H(0) = \delta_4, \theta'(0) = \delta_5$ and $\theta_p(0) = \delta_6$. Let $\delta_i (i = 1, 2, 3, 4, 5, 6)$ be the correct values of $f''(0)$, $F(0)$, $G(0)$, $H(0)$, $\theta'(0)$ and $\theta_p(0)$. We integrate the resulting system of nine ordinary differential equations using the fourth-order Runge–Kutta method and obtain the values of $f''(0)$, $F(0)$, $G(0)$, $H(0)$, $\theta'(0)$ and $\theta_p(0)$. The solution process is repeated with another larger value of η_∞ until two successive values of $f''(0)$, $F(0)$, $G(0)$, $H(0)$, $\theta'(0)$ and $\theta_p(0)$ differ only after desired digit signifying the limit of the boundary along η. The last value of η_∞ is chosen as the appropriate value for that particular set of parameters. Finally, the problem can be solved numerically using a second-order finite difference scheme known as the Keller-box method. The numerical solutions are obtained in four steps as follows:

- Reduce the system (11) to a system of first order equations.
- Write the difference equations using central differences.
- Linearize the algebraic equations by Newton's method, and write them in matrix-vector form.
- Solve the linear system by the block tri-diagonal elimination technique.

For the sake of brevity, the details of the numerical procedure are not presented here. It is also important to note that the computational time for each set of input parameters should be short. Because physical domain in this problem is unbounded, whereas the computational domain has to be finite, we apply the far field boundary conditions for the similarity variable η at finite value denoted by η_{max}. We ran our bulk of computations with the value $\eta_{max} = 7$, which is sufficient to achieve the far field boundary conditions asymptotically for all values of the parameters considered. For numerical calculations, a uniform step size of $\Delta \eta = 0.01$ is found to be satisfactory and the solutions are obtained with an error tolerance of 10^{-6} in all the cases. The accuracy of the numerical scheme is validated by comparing the skin friction and the rate of heat transfer results with those available in the literature: They agree very well (see Tables 1 and 2).

4. Graph
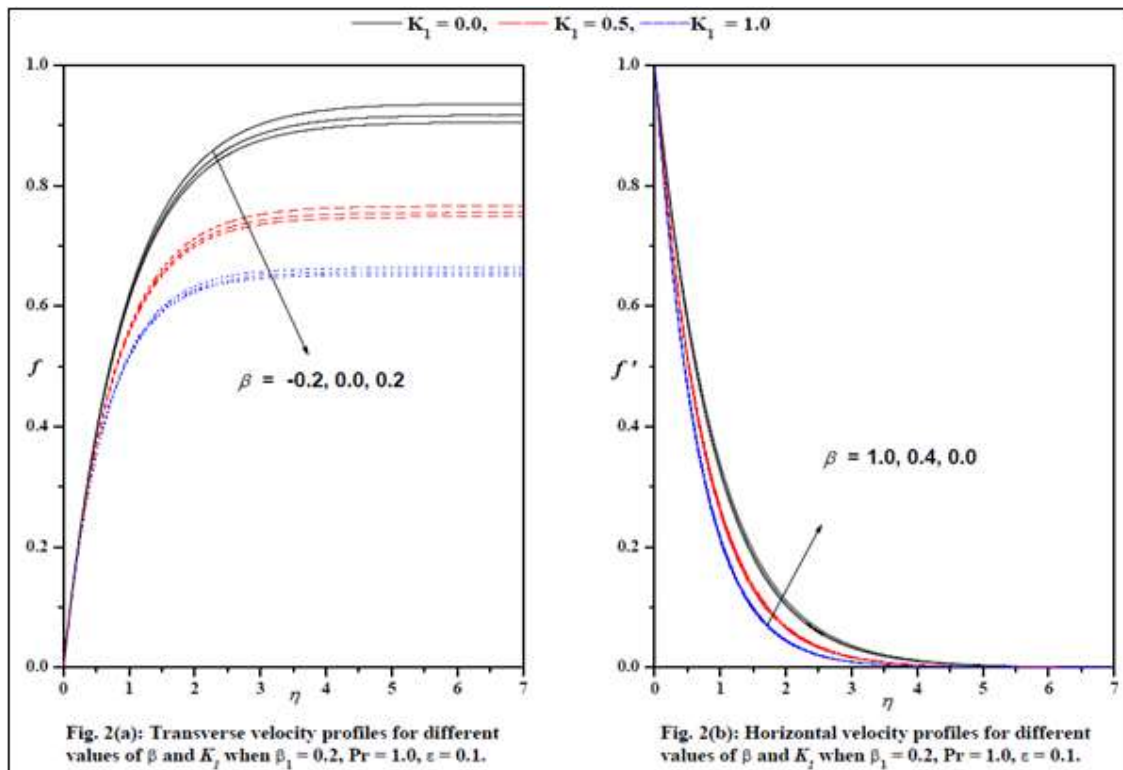
Fig. 2(a): Transverse velocity profiles for different values of β and K_l when $\beta_1 = 0.2$, Pr = 1.0, ε = 0.1.

Fig. 2(b): Horizontal velocity profiles for different values of β and K_l when $\beta_1 = 0.2$, Pr = 1.0, ε = 0.1.

Fig. 2(c): Particle velocity components *F* for different values of β and K_1 when $β_1 = 0.2$, Pr = 1.0, ε = 0.1.

Fig. 2(d): Particle velocity components *G* for different values of β and K_1 when $β_1 = 0.2$, Pr = 1.0, ε = 0.1.

Fig. 3(a): Transverse velocity profiles for different values of $β_1$ and K_1 when β = 0.2, Pr = 1.0, ε = 0.1.

Fig. 3(b): Horizontal velocity profiles for different values of $β_1$ and K_1 when β = 0.2, Pr = 1.0, ε = 0.1.

Fig. 3(c): Particle velocity components F for different values of β_1 and K_1 when $\beta = 0.2$, Pr = 1.0, $\varepsilon = 0.1$.

Fig. 3(d): Particle velocity components G for different values of β_1 and K_1 when $\beta = 0.2$, Pr = 1.0, $\varepsilon = 0.1$.

Fig. 4(a): Fluid temperature profiles for different values of β and K_1 when $\beta_1 = 0.2$, Pr = 1.0, $\varepsilon = 0.1$.

Fig. 4(b): Dust-phase temperature profiles for different values of β and K_1 when $\beta_1 = 0.2$, Pr = 1.0, $\varepsilon = 0.1$.

Fig. 5(a): Fluid temperature profiles for different values of β_1 and K_1 when $\beta = 0.2$, $Pr = 1.0$, $\varepsilon = 0.1$.

Fig. 5(b): Dust-phase temperature profiles for different values of β_1 and K_1 when $\beta = 0.2$, $Pr = 1.0$, $\varepsilon = 0.1$.

Fig. 6(a): Fluid temperature profiles for different values of ε and Pr when $\beta = 0.2$, $K_1 = 0.5$, $\beta_1 = 0.2$.

Fig. 6(b): Dust-phase temperature profiles for different values of ε and Pr when $\beta = 0.2$, $K_1 = 0.5$, $\beta_1 = 0.2$.

5. Discussion of the Results

In this section, we illustrate the effects of the pertinent parameters, namely, the fluid-particle interaction parameter β, the Maxwell parameter β_1, the permeability parameter K_1, the variable thermal conductivity parameter ε, and the Prandtl number Pr on the flow and heat transfer of the UCM fluid over a horizontal stretching sheet. The temperature relaxation parameter L_0 is chosen to be unity throughout the computation. In order to analyze the salient features of the problem, the numerical results are illustrated graphically in Figs. 2-6. Also the numerical results for the skin friction, the particle velocity and the density components, the fluid temperature, and the dust-phase temperature at the surface for different values of the physical parameters are recorded in Table 3.

The transverse velocity $f(\eta)$, the horizontal velocity $f'(\eta)$, the particle transverse velocity $F(\eta)$ and the particle horizontal velocity $G(\eta)$ profiles are shown in Figs. 2(a)–2(d) for different values of K_1 and β. The general trend is that $f'(\eta)$, $F(\eta)$ and $G(\eta)$ decrease monotonically as the distance increases from the surface, whereas $f(\eta)$ increases as the distance increases from stretching sheet. It is observed from these figures that $f'(\eta)$ and $F(\eta)$ profiles decrease with an increase in K_1. This observation holds true even with particle velocity component $F(\eta)$; but quite the opposite is true with $G(\eta)$. Physically it means that the permeability parameter (normal to the flow direction) has a tendency to induce a drag, which tends to resist the flow. It is noticed that the effect of increasing values of β is to

reduce the thickness of the fluid velocity in the boundary layer and increase the dust-phase transverse velocity, as well as the horizontal velocity component.

Figs. 3(a)-3(d) exhibit the transverse velocity $f(\eta)$, the horizontal velocity $f'(\eta)$, the particle transverse velocity $F(\eta)$ and the particle horizontal velocity $G(\eta)$ profiles for several sets of values of K_1 and β_1. The effect of the permeability of the porous medium on the velocity of the fluid elements above the sheet appears to become less pronounced for the Maxwell fluid, i.e., by an increase in the elasticity level of the fluid. That is to say that larger velocity can be expected to arise in porous medium over stretching sheets if the fluid is elastic. It is evident from the Figs. 3(a)-3(d) that the effect of increasing values of the Maxwell parameter is to reduce the fluid velocity in the boundary layer and the dust-phase horizontal velocity, but quite opposite is found in dust-phase transverse velocity.

Figures 4-6 show the fluid temperature $\theta(\eta)$ and dust-phase temperature $\theta_p(\eta)$ profiles for different values of the governing parameters. The general trend is that the fluid-temperature distribution is unity at the surface, whereas the dust-phase temperature is not. However, with the changes in the governing parameters both asymptotically tend to zero as the distance increases from the boundary. Figs.4(a) and 4(b) illustrate the effect of K_1 and β on $\theta(\eta)$. The effect of increasing values of Mn is to increase $\theta(\eta)$ and also $\theta_p(\eta)$. From the graphical representation, the magnetic field has a significant effect on the temperature field. As explained above, the permeability parameter gives rise to a resistive force. This force makes the fluid experience a resistance by increasing the friction between its layers. Hence, there is an increase in the temperature profile as well as the dust-phase profile. The effect of β is to decrease the temperature profile that in turn reduces the thickness of the thermal boundary, whereas it enhances the dust-phase temperature at the surface: Thus increases the thickness of the dust-phase temperature.

Figs. 5(a) and 5(b) exhibit the fluid-temperature distribution and the dust-phase temperature distribution for several sets of values of the K_1 and β_1. The effect of the porosity parameter on the temperature field is less significant for Maxwell fluid, i.e., for elastic liquids. The effect of β_1 is to increase the fluid temperature and the dust-phase temperature. This is due to the fact that the thickening of the thermal boundary layer occurs due to an increase in the elasticity stress parameter. However, the temperature distribution asymptotically tends to zero as the distance increases from the boundary. The graphs for $\theta(\eta)$ and $\theta_p(\eta)$ for different values of ε and Pr are, shown in Figs. 6(a) and 6(b). These figures demonstrate that an increase in ε results in an increase in the temperature $\theta(\eta)$ as well as in $\theta_p(\eta)$. This is due to the fact that

the assumption of temperature dependent thermal conductivity implies a reduction in the magnitude of the transverse velocity by a quantity $\partial K(T)/\partial y$ as can be seen from the energy equation. Also, we observe that the effect of Pr is to decrease both $\theta(\eta)$ and $\theta_p(\eta)$. Finally, the effects of all the physical parameters on the surface-velocity gradient, the particle-velocity components, particle-density component, the temperature gradient, and the dust-phase temperature at the sheet are presented in Table 3. It is of interest to note that the effect β_1, K_1 and β is to increase the magnitude of the skin friction coefficient. However, the effect of $\varepsilon, \beta_1,$ and K_1 is to decrease the magnitude of the temperature gradient at the sheet; but the reverse trend is observed with an increase in Pr and β. From Table 3, it is further noticed that the effect of K_1 and β is to increase the dust-phase temperature and the particle velocity component.

6. Conclusion

Some of the interesting observations are:
- The effect of increasing values of the fluid-particle interaction parameter, Maxwell parameter and the porosity parameter is to decrease the velocity throughout the boundary layer.
- The effect of increasing values of the fluid-particle interaction parameter is to reduce the fluid temperature. However, quite opposite is found in particle phase temperature.
- The effect of the Maxwell parameter, the porosity parameter and the variable thermal conductivity parameter is to enhance the fluid temperature and the particle phase temperature in the flow region.
- The thermal boundary layers of the fluid and the dust phase are significantly influenced by the Prandtl number. The effect of Pr is to decrease the thermal boundary layer thickness.

References

[1] B.C. Sakiadis, Boundary-layer behavior on continuous solid surfaces I, The boundary layer on a equations for two dimensional and axisymmetric flow, A.I.Ch.E.J. 7 (1961) 26-28.

[2] L.J. Crane, Flow past a stretching plate, ZAMP 1 (1970) 645-647.

[3] L.G. Grubka, K.M. Bobba, Heat transfer characteristics of a continuous stretching surface with variable temperature, ASME J. Heat Transf. 107 (1985) 248–250.

[4] B.K. Dutta, P. Roy, A.S. Gupta, Temperature field in flow over a stretching sheet with uniform heat flux, Int. Comm. Heat Mass Transf. 12 (1985) 89-94.

[5] C.K. Chen, M.I. Char, Heat transfer of a continuous stretching surface with suction or blowing, J. Math. Anal. Appl. 135 (1988) 568-580.

[6] M.E. Ali, Heat transfer characteristics of a continuous stretching surface, Heat Mass Transf. 29 (1994) 227–234.

[7] A. Ishak, R. Nazar, I. Pop, Boundary layer flow and heat transfer over an unsteady stretching vertical surface, Meccanica 44 (2009) 369–375.

[8] Subhas, A., and P. Veena. "Visco-elastic fluid flow and heat transfer in a porous medium over a stretching sheet." International journal of non-linear mechanics 33.3 (1998): 531-540.

[9] Chakrabarti, A., and A. S. Gupta. "Hydromagnetic flow and heat transfer over a stretching sheet." Quarterly of Applied Mathematics 37.1 (1979): 73-78.

[10] Zheng, Liancun, Chaoli Zhang, Xinxin Zhang, and Junhong Zhang. "Flow and radiation heat transfer of a nanofluid over a stretching sheet with velocity slip and temperature jump in porous medium." Journal of the Franklin Institute 350, no. 5 (2013): 990-1007.

[11] Prasad, K. V., Subhas Abel, and P. S. Datti. "Diffusion of chemically reactive species of a non-Newtonian fluid immersed in a porous medium over a stretching sheet." International Journal of Non-Linear Mechanics 38.5 (2003): 651-657.

[12] Khan, Noor Saeed, Saeed Islam, Taza Gul, Ilyas Khan, Waris Khan, and Liaqat Ali. "Thin film flow of a second grade fluid in a porous medium past a stretching sheet with heat transfer." Alexandria Engineering Journal 57, no. 2 (2018): 1019-1031.

[13] Makinde, O. D., Z. H. Khan, R. Ahmad, and W. A. Khan. "Numerical study of unsteady hydromagnetic radiating fluid flow past a slippery stretching sheet embedded in a porous medium." Physics of Fluids 30, no. 8 (2018): 083601.

[14] Ullah, Imran, Sharidan Shafie, and Ilyas Khan. "Effects of slip condition and Newtonian heating on MHD flow of Casson fluid over a nonlinearly stretching sheet saturated in a porous medium." Journal of King Saud University-Science 29.2 (2017): 250-259.

[15] Jafar, Ahmad Banji, Sharidan Shafie, and Imran Ullah. "MHD radiative nanofluid flow induced by a nonlinear stretching sheet in a porous medium." Heliyon 6.6 (2020): e04201.

[16] Nayak, M. K. "Chemical reaction effect on MHD viscoelastic fluid over a stretching sheet through porous medium." Meccanica 51.8 (2016): 1699-1711.

[17] Hayat, T., M. Imtiaz, A. Alsaedi, and R. Mansoor. "MHD flow of nanofluids over an exponentially stretching sheet in a porous medium with convective boundary conditions." Chinese Physics B 23, no. 5 (2014): 054701.

[18] Mukhopadhyay, Swati, and G. C. Layek. "Effects of variable fluid viscosity on flow past a heated stretching sheet embedded in a porous medium in presence of heat source/sink." Meccanica 47.4 (2012): 863-876.

[19] Jabeen, K., M. Mushtaq, and R. M. Akram. "Analysis of the MHD boundary layer flow over a nonlinear stretching sheet in a porous medium using semianalytical approaches." Mathematical Problems in Engineering 2020 (2020).

[20] Mohanty, B., S. R. Mishra, and H. B. Pattanayak. "Numerical investigation on heat and mass transfer effect of micropolar fluid over a stretching sheet through porous media." Alexandria Engineering Journal 54, no. 2 (2015): 223-232.

[21] P.G. Saffman, On the stability of laminar flow of a dusty gas, J. Fluid. Mech.13 (1962) 120-128.

[22] N. Datta, S.K. Mishra, Boundary layer flow of a dusty fluid over a semi-infinite flat plate, Acta Mech.42 (1982) 71-83.

[23] K. Vajravelu, J. Nayfeh, Hydromagnetic flow of a dusty fluid over a stretching sheet, Int. J. Non-linear Mech.27 (1992) 937-945.

[24] Xie Ming-Liang, Lin Jian-Zhong, Xing Fu-Tang, On the hydrodynamic stability of a particle-laden flow in growing flat plate boundary layer, J. Zhejiang Uni. SCI. A 8 (2007) 275-284.

[25] K. Vajravelu, K.V. Prasad, P.S. Datti, Hydromagnetic fluid flow and heat transfer at a stretching sheet with fluid-particle suspension and variable fluid properties, Journal of Fluids Engineering 134 (2012) 121001-3.

[26] T.C. Chiam, Heat transfer in a fluid with variable thermal conductivity over a stretching sheet, Acta Mech. 29 (1998) 63-72.

[27] K. Vajravelu, K.V. Prasad, S.R. Santhi, Axisymmetric magneto-hydrodynamic (MHD) flow and heat transfer at a non-isothermal stretching cylinder, Applied Mathematics and Computation 219 (2012) 3993–4005.

[28] T. Cebeci, P. Bradshaw, Physical and computational aspects of convective heat transfer, Springer-Verlag, New York, 1984.

[29] H.B. Keller, Numerical Methods for Two-point Boundary Value Problems, Dover Publ., New York 1992.

[30] H.I. Andersson, K.H. Bech, B.S. Dandapat, Magneto-hydrodynamic flow of a power law fluid over a stretching sheet, Int J Non-Linear Mech. 27 (1992) 929–936.

Table 1: Comparison of some of the values of $-f''(0)$ when $\beta = 0.0, \ \Pr = 1.0.$ and $\varepsilon = 0.0$.

When $\beta_1 = 0.0$	$K_1 = 0.0$	$K_1 = 0.5$	$K_1 = 1.0$	$K_1 = 1.5$	$K_1 = 2.0$
Andersson et al. [30] for n=1	1.00000	1.2249	1.4140	1.58100	1.73200
Prasad et al. [20]	1.000174	1.224753	1.414499	1.581139	1.732203
Present results	1.000174	1.22475	1.41421	1.58114	1.73205
When $Mn = 0.0$	$\beta_1 = 0.0$	$\beta_1 = 0.2$	$\beta_1 = 0.4$	$\beta_1 = 0.6$	$\beta_1 = 0.8$
Sadeghy [17]	1.00000	1.0549	1.10084	1.0015016	1.19872
Vajravelu et al.[19]	1.0001743	1.051975	1.1019475	1.1501625	1.1967279
Present results	1.000174	1.05198	1.10195	1.15016	1.19673

Table 2: Comparison of some of the values of $-\theta'(0)$ when $\beta = 0.0$, $K_1 = 0.0$ and $\varepsilon = 0.0$.

When $\beta_1 = 0.0$	Pr = 0.72	Pr = 1.0	Pr = 3.0	Pr = 6.7	Pr = 10.0
Grubkha and Bobba [3]	0.8086	1.0000	1.9237	-	3.7207
Ali [6]	0.8058	0.9961	1.9144	-	3.7006
Ishak et al. [7]	0.8086	1.0000	1.9237	3.0003	3.7207
Present results	0.808836	1.000000	1.923687	3.000272	3.720788
When Pr = 1.0	β_1 = 0.0	β_1 = 0.2	β_1 = 0.4	β_1 = 0.6	β_1 = 0.8
Vajravelu et al.[19]	1.0001743	0.9800923	0.9607879	0.9423181	0.9246983
Present results	1.000174	0.9800925	0.9607877	0.9423183	0.9246984

Table 3: Numerical values for skin friction $f''(0)$, the particle velocity components $F(0), G(0)$, the particle density component $H(0)$, the wall temperature gradient $\theta(0)$, and the wall temperature dust particles $\theta_p(0)$ for different values of the physical parameters.

Pr	ε	β_1	K_1	β	$f''(0)$	$F(0)$	$G(0)$	$H(0)$	$\theta'(0)$	$\theta_P(0)$
1.0	0.1	0.2	0.0	0.0	-1.05198	0.00000	-0.91721	0.20000	-0.91331	0.00000
				0.2	-1.06772	0.16766	-0.74287	0.20335	-0.97889	0.12794
				1.0	-1.10203	0.52204	-0.30747	0.26545	-1.11558	0.41699
			0.5	0.0	-1.28079	0.00000	-0.75534	0.20000	-0.85530	0.00000
				0.2	-1.29379	0.16766	-0.61388	0.20335	-0.92853	0.16030
				1.0	-1.32234	0.52206	-0.25620	0.26541	-1.06476	0.45086
			1.0	0.0	-1.47454	0.00000	-0.65650	0.20000	0.80837	0.00000
				0.2	-1.48586	0.16766	-0.53473	0.20335	-0.88773	0.18858
				1.0	-1.51082	0.52207	-0.22422	0.26538	-1.02239	0.47543
1.0	0.1	0.0	0.5	0.0	-1.22475	0.00000	-0.81593	0.20000	-0.87683	0.00000
				0.2	-1.23838	0.16746	-0.66061	0.20341	-0.94702	0.14696
				1.0	-1.26830	0.52143	-0.27293	0.26617	-1.08360	0.43885
		0.2	0.5	0.0	-1.28079	0.00000	-0.75534	0.20000	-0.85530	0.00000
				0.2	-1.29379	0.16766	-0.61388	0.20335	-0.92853	0.16030
				1.0	-1.32234	0.52206	-0.25620	0.26541	-1.06476	0.45086
		1.0	0.5	0.0	-1.48979	0.00000	-0.59761	0.20000	-0.77975	0.00000
				0.2	-1.50079	0.16813	-049030	0.20319	-0.86330	0.20926
				1.0	-1.52507	0.52368	-0.20987	0.26349	-0.99637	0.48877
1.0	0.0	0.2	0.5	0.0	-1.28083	0.00000	-0.75394	0.20000	-0.92319	0.00000
				0.2	-1.29379	0.16766	-0.61381	0.20335	-0.99709	0.15460
				1.0	-1.32237	0.52207	-0.25617	0.26537	-1.14308	0.44341
	0.2	0.2	0.5	0.0	-1.28083	0.00000	-0.75394	0.20000	-0.80431	0.00000
				0.2	-1.29379	0.16766	-0.61381	0.20335	-0.87099	0.16510
				1.0	-1.32237	0.52207	-0.25617	0.26537	-1.00004	0.45719
	0.4	0.2	0.5	0.0	-1.28083	0.00000	-0.75394	0.20000	-0.71619	0.00000
				0.2	-1.29379	0.16766	-0.61381	0.20335	-0.77751	0.71511
				1.0	-1.32237	0.52207	-0.25617	0.26537	-0.89403	0.46915
0.72	0.1	0.2	0.2	0.0	-1.22475	0.00000	-0.81593	0.20000	-0.70200	0.00000
				0.2	-1.29379	0.16766	-0.61381	0.20335	-0.76722	0.24194
				1.0	-1.28833	0.70817	-0.06469	0.52063	-0.90682	0.54564
1.0	0.1	0.2	0.2	0.0	-1.22475	0.00000	-0.81593	0.20000	-0.87683	0.00000
				0.2	-1.29379	0.16766	-0.61381	0.20335	-0.92890	0.15991
				1.0	-1.28833	0.70817	-0.06469	0.52063	-1.08360	0.43885
2.0	0.1	0.2	0.2	0.0	-1.22475	0.00000	-0.81593	0.20000	-1.36681	0.00000
				0.2	-1.29379	0.16766	-0.61381	0.20335	-1.39216	0.05796
				1.0	-1.28833	0.70817	-0.06469	0.52063	-1.54268	0.23531
5.0	0.1	0.2	0.2	0.0	-1.22475	0.00000	-0.81593	0.20000	-2.33917	0.00000
				0.2	-1.29379	0.16766	-0.61381	0.20335	-2.34460	0.01386
				1.0	-1.28833	0.70817	-0.06469	0.52063	-2.45253	0.08022
10.0	0.1	0.2	0.2	0.0	-1.22475	0.00000	-0.81593	0.20000	-3.43155	0.00000
				0.2	-1.29379	0.16766	-0.61381	0.20335	-3.42930	0.00473
				1.0	-1.28833	0.70817	-0.06469	0.52063	-3.50713	0.03229